ADVANCED ENERGY MATERIALS
www.advenergymat.de

Unlocking Stable Multi-Electron Cycling in NMC811 Thin-Films between 1.5 – 4.7 V

Abdessalem Aribia, Jordi Sastre, Xubin Chen, Moritz H. Futscher, Matthias Rumpel, Agnieszka Priebe, Max Döbeli, Nicolas Osenciat, Ayodhya N. Tiwari, and Yaroslav E. Romanyuk*

Among cathode materials, $LiNi_{0.8}Mn_{0.1}Co_{0.1}O_2$ (NMC811) is the most discussed for high performance Li-ion batteries, thanks to its capacity of ≈200 mAh g^{-1} and low Co content. Here, it is demonstrated that NMC811 can reversibly accommodate more than one Li-ion per formula unit when coupled with a solid-state electrolyte, thus significantly increasing its capacity. Sputtered Li-rich NMC811 cathodes are tested with lithium–phosphorus–oxynitride as a solid-state electrolyte in a thin-film architecture, which is a simplified 2D model with direct access to the cathode-electrolyte interface. The solid-state electrolyte helps to stabilize the interface and prevents capacity fading, voltage decay, and interface resistance growth, thus allowing cycling at extended voltage ranges of 1.5–4.7 V. While the liquid electrolyte cells suffer from rapid capacity decay, the Li-rich NMC811 cells with the solid-state electrolyte can cycle at a fast rate and an initial capacity of 149 mAh g^{-1} from 1.5 to 4.3 V for 1000 cycles. The all-solid-state thin-film cells with a lithium metal anode yield a discharge capacity of up to 350 mAh g^{-1} at C/10 because of multi-electron cycling with a coulombic efficiency of 90.1%. The results demonstrate how solid-state electrolytes that are stable against NMC811 cathodes can unlock the full potential of this Li-rich and Ni-rich cathode class.

1. Introduction

The demand for lithium-ion batteries for electric vehicles is projected to expand nearly tenfold by 2030.[1] Not only the market volume but also the gravimetric and volumetric density of batteries is expected to improve, thus accelerating the global spread e-mobility and enabling new applications such as eVTOLs. The cathode is a bottleneck in further increasing the energy densities of lithium-ion batteries because the reversible capacity of current cathodes is lower than that of conventional graphite anodes (372 mAh g^{-1}) and far behind that of high-capacity anodes such as lithium metal (3860 mAh g^{-1}) and silicon (4200 mAh g^{-1}).[2,3] Simultaneously, the cathode is the main contributor to the material cost at the cell level.[4] Currently, $LiNi_{0.8}Mn_{0.1}Co_{0.1}O_2$ (NMC811) is gaining commercial adoption due to its capacity of ≈200 mAh g^{-1} assuming one Li-ion per formula unit and low content of expensive cobalt.[5] Two intriguing research questions stand out: i) Is it possible to increase the cathodic discharge capacity by introducing additional lithium into the host NMC811 structure? ii) Can we control the reactivity of Ni-rich cathode material with the electrolyte and prevent the formation of a solid electrolyte interphase (SEI) layer and consequent low capacity retention?[6,7] NMC cathodes can actually store more than one lithium ion per formula unit. This phenomenon is by no means a recent discovery, and the first reports of Li-rich NMC-type layered oxide cathodes date back to 2003.[8]

When discussing Li-rich layered cathode materials, it is important to differentiate between Mn-based and Ni-based compositions. Most of the investigated Li-rich NMC compounds are based on Mn as main redox-active transition metal.[9,10] This allows for excess lithium to be stored in a Li_2MnO_3 composite structure embedded in Li(Ni, Mn, Co)O_2, where oxygen atoms are involved in the redox process above 4.5 V.[11] Such

A. Aribia, J. Sastre, X. Chen, M. H. Futscher, N. Osenciat, A. N. Tiwari, Y. E. Romanyuk
Laboratory for Thin Films and Photovoltaics
Empa – Swiss Federal Laboratories for Materials Science and Technology
Überlandstrasse 129, Dübendorf CH-8600, Switzerland
E-mail: abdessalem.aribia@empa.ch

The ORCID identification number(s) for the author(s) of this article can be found under https://doi.org/10.1002/aenm.202201750.

DOI: 10.1002/aenm.202201750

M. Rumpel
Fraunhofer R&D Center for Electromobility
Fraunhofer ISC
Neunerplatz 2, 97082 Würzburg, Germany

A. Priebe
Laboratory for Mechanics of Materials and Nanostructures
Empa - Swiss Federal Laboratories for Materials Science and Technology
Feuerwerkerstrasse 39, Thun CH-3602, Switzerland

M. Döbeli
Ion Beam Physics
ETH Zürich - Swiss Federal Institute of Technology
Otto-Stern-Weg 5, Zürich CH-8093, Switzerland

overlithiated Mn-rich cathodes with an appropriate doping and coating can yield capacities over 200 mAh g^{-1} for several hundred cycles.[12,13]

Fewer reports exist on Li-rich and Ni-rich cathodes. Pure $LiNiO_2$ can be overlithiated to reach a theoretical capacity of 513 mAh g^{-1}, yet capacity fades during the first cycles because of irreversible O_2 release.[14–18]

For ternary Ni-rich materials such as NMC622 and NMC811, additional lithium can be chemically or electrochemically introduced to the cathode after fabrication. To date, attempts to intercalate more than one lithium per formula unit were limited to one cycle. Electrochemically overlithiated Ni-rich NMC showed capacities of up 550 mAh g^{-1} but only for one cycle.[19] In other studies, chemically overlithiated NMC cathodes were used to compensate for the lithium loss in anode-free cells during the first cycle.[20]

Another underlying challenge of Ni-rich cathode materials such as NMC811 is chemically reactive $Ni^{3+/4+}$ ions, which react with liquid organic electrolytes during battery cycling to form a resistive cathode-electrolyte interface. The cathode-electrolyte interface is crucial for the performance of NMC811, where the cathode material undergoes surface degradation to undesirable rock-salt and disordered spinel phases. Several different strategies have been employed to control the reactivity of NMC811 with liquid organic electrolytes. Among the most popular methods, doping the cathode bulk material[21,22] and introducing an additional cathode coating at the cathode-electrolyte interface are employed.[23–25] Although several hundred cycles have been achieved with various doping and coating approaches,[22,23] these strategies incur increased processing costs. Furthermore, NMC811 cathodes tend to expand anisotropically during delithiation, resulting in cracks, which electrically isolate parts of the NMC811 cathode.[11]

This study addresses both interconnected questions of Li-rich and Ni-rich layered cathode materials and demonstrates Li-rich NMC811 that reversibly stores more than one Li-ion per formula unit. Lithium–phosphorus–oxynitride (LiPON) is chosen as a well-established solid-state electrolyte and because of its compatibility with high voltage NMC811 cathodes and lithium metal.[26] A 10-nm LiPON coating was previously used with Li-rich Mn-based $Li_{1.2}Mn_{0.525}Ni_{0.175}Co_{0.1}O_2$ by by Martha et al.[27] to improve the capacity retention to ≈250 mAh g^{-1} after 300 cycles at C/10. In addition, LiPON can compensate for cathode volume changes due to its amorphous nature, which is important in conjunction with Li-rich cathode materials. To take full advantage of Li-rich NMC811, cycling at extended voltages of 1.5–4.7 V is necessary. To elucidate the reactivity of the interface, we employ a thin-film model system. The main advantage of the thin-film configuration over conventional battery geometries is that neither conductive additives nor binders are present in the cathode. Therefore, thin-film systems offer reduced complexity and direct access to the isolated cathode-electrolyte interface, making them an attractive choice for exploring interfacial phenomena.[28] A process for magnetron-sputtered Li-rich NMC811 thin films was developed. The capacity and cycling performance of the solid-state cells was compared to that of cells with liquid organic electrolyte. It was found that changing from a liquid to a solid electrolyte mitigated interfacial degradation, allowing capacities up to 350 mAh g^{-1} during the first cycle at C/10. The solid-electrolyte cathode interface allowed for stable cycling over 1000 cycles at 4 C with an initial capacity of 149 mAh g^{-1}.

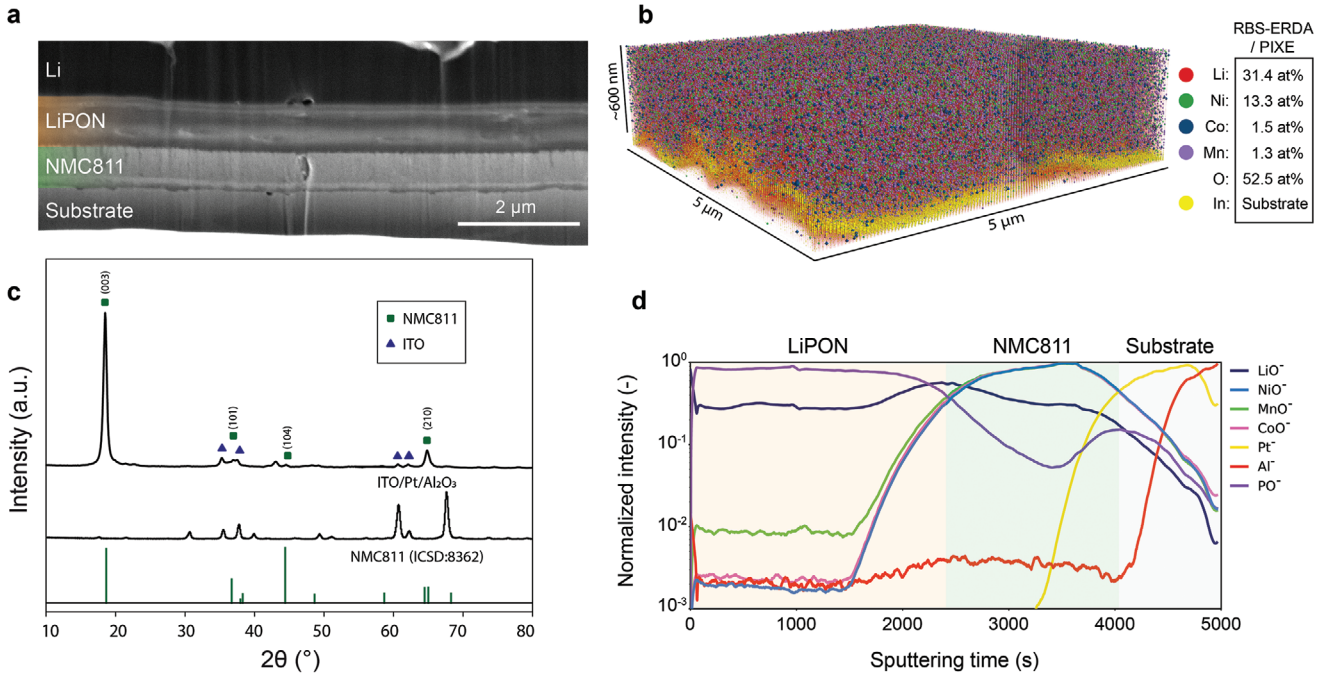

Figure 1. a) Cross-section SEM image of the all-solid-state battery stack (Li/LiPON/NMC811/Pt/Ti/sapphire) b) Elemental tomogram obtained by FIB-ToF-SIMS of an Li-rich NMC811 film with composition obtained from RBS-ERDA and PIXE measurements. c) Grazing-incidence XRD patterns of the annealed NMC811/ITO/Pt/Al_2O_3 stack, ITO/Pt/Al_2O_3 substrate, and ICSD reference for NMC811. d) ToF-SIMS depth profile of an all-solid-state battery stack after annealing.

2. Results and Discussion

Li-rich NMC811 films were deposited on ITO-coated stainless steel substrates by magnetron sputtering from an overlithiated $Li_{1.6}Ni_{0.8}Mn_{0.1}Co_{0.1}O_2$ target at room temperature with subsequent annealing at 600 °C. All-solid-state cells were prepared by sputtering LiPON as an electrolyte on the Li-rich NMC811 films and then evaporating metallic lithium on top. The cross-section of the all-solid-state thin-film stack (**Figure 1**a) exhibits sharp interfaces, which are a distinctive characteristic of thin-film systems, and a characteristic columnar microstructure perpendicular to the substrate of NMC811 after heat treatment. In contact with metallic lithium, LiPON degrades to Li_3N, Li_2O, and Li_3PO_4,[29] causing an additional layer to appear in the cross section. The poor electronic conductivity of the decomposition products inhibits further electrolyte degradation.

To investigate the elemental structure and distribution, a 3D tomogram in Figure 1b displays the interior of the NMC811 film reconstructed from a gas-assisted focused ion beam time of flight secondary ion mass spectrometry (FIB-ToF-SIMS) measurement (Figure 1b). The measurement shows a uniform distribution of the transition metal elements. An overlithiated target was used for Li-rich NMC811 sputtering to compensate for lithium loss during deposition and crystallization at high temperatures, a notorious problem in thin-film cathode fabrication. Remarkably, RBS-ERDA and PIXE measurements indicated that not only lithium loss was prevented, but a large excess of lithium was present in the NMC811 cathode after crystallization, resulting in a composition of $Li_{1.95}Ni_{0.83}Mn_{0.08}Co_{0.09}O_{xx}$. (The oxygen content cannot be given precisely due to the ITO layer below the thin-film cathode.) The higher Li content of sputtered thin films compared to the target is due to the sputter yield amplification effect. This effect describes an increase in the sputter yield of light elements sputtered from a composite target.

The crystallinity of the Li-rich NMC811 films was evaluated by grazing-incidence X-ray diffractometry (GI-XRD). The XRD pattern of the full stack of annealed 600 nm NMC811/ITO/Pt/Al_2O_3 contains reflexes of the underlying ITO/Pt/Al_2O_3 substrate and a few additional reflections (Figure 1c). The strong signal at 18° can be attributed to the (003) reflex of layered R-3m type structure of crystallized transition metal oxide cathode films.[30] A high degree of preferred orientation or texturing with the c axes of most grains normal to the substrate is observed.[31] The (003) reflex angle coincides with the ICSD(8362) reference for NMC811 and is not shifted to lower angles as would be expected from higher c-spacing due to additional lithium intercalation.[20] Therefore we cannot exclude the presence of Li-rich segregations, which are below the resolution of the XRD measurement. The interface between NMC811 and the LiPON solid-state electrolyte was further investigated with time-of-flight secondary ion mass spectrometry (ToF-SIMS), as shown in Figure 1d. The signals corresponding to NiO–, MnO–, and CoO– are well correlated, indicating no segregation of transition metal oxides across the cathode film.

We tested the electrochemical performance of Li-rich NMC811 in half-cell measurements with an organic liquid electrolyte (**Figure 2**a) and compared it to all-solid-state cells with LiPON as the electrolyte (Figure 2b). Half-cell measurements differ from conventional full cells in that they operate with a

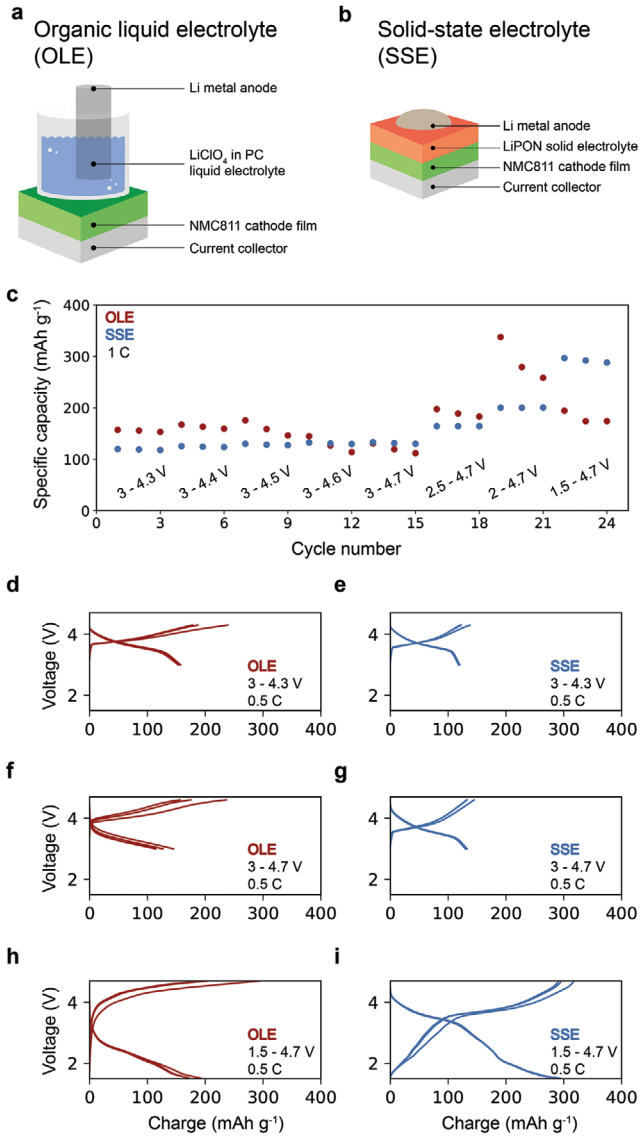

Figure 2. a) Schematic illustration of the NMC811 cathode investigated in a two-electrode half-cell configuration. b) Solid-state electrolyte cell with the NMC811 cathode and LiPON electrolyte. c) Capacity of the cells with liquid (OLE, red) and solid (SSE, blue) electrolytes over different voltage ranges at 1 C. d–i) Charge–discharge curves of liquid (left) and solid electrolyte cells (right) over selected voltage ranges at C/2.

significant excess of electrolyte and lithium, as in this work, representing an idealized system where a low coulombic efficiency can be compensated by an infinite lithium and electrolyte reservoir. Therefore, a longer cycle life and higher robustness towards side reactions are expected in a half-cell setup than in conventional cells. $LiClO_4$ in propylene carbonate (PC) was used as a liquid electrolyte in this work because of the absence of corrosive HF contaminants that are inevitably present in $LiPF_6$ solutions.[32] When a more conventional $LiPF_6$ in EC:DMC liquid electrolyte was used to cycle the Li-rich NMC811 cathodes, an initial capacity of only only 80 mAh g^{-1} was observed, and the capacity deteriorated in the first few cycles (Figure S1, Supporting Information). No external pressure was

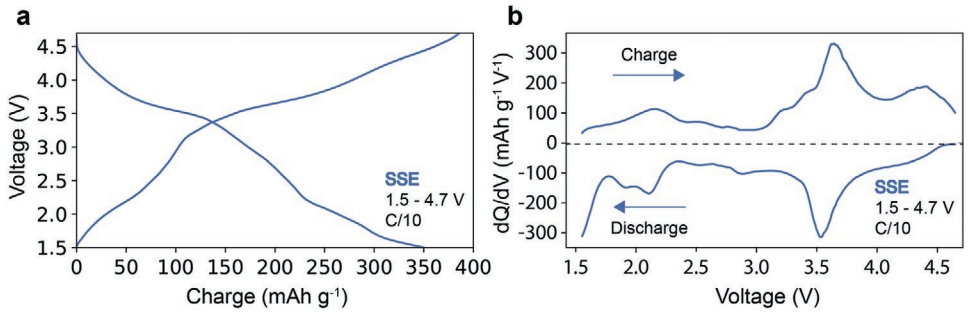

Figure 3. a) First cycle charge-discharge curve for the NMC811 solid-state electrolyte cell cycled from 1.5 to 4.7 V at C/10. b) Corresponding differential capacity versus voltage (dQ/dV) curves.

applied to the cells, and all measurements were performed at room temperature.

Figure 2c compares the discharge capacity of Li-rich NMC811 with the liquid electrolyte and the solid electrolyte cycled at different potentials. First, the upper cut-off voltage was raised stepwise from 4.3 to 4.7 V, whereas the lower voltage was kept stable at 3.0 V versus Li/Li^+ while cycling at 1 C (= 40 μ A cm^{-2}). Raising the upper cut-off voltage had no pronounced effect on the discharge capacity in either electrolyte system. For Li-rich NMC811 cathodes measured with liquid electrolyte, an increase in capacity from 160 to 180 mAh g^{-1} at 4.5 V is observed. Further increase in the voltage to 4.7 V leads to a decrease in cathode capacity to 130 mAh g^{-1}. These capacities are low compared to bulk NMC811, which usually achieves capacities of 200 mAh g^{-1} when cycled between 3 and 4.3 V.[5] However, in thin-film geometry, interfacial degradation is exacerbated due to increased interface to bulk ratio and thus leads to a lower capacity compared to bulk NMC811. The values observed are similar to previously reported thin-film NMC type cathodes.[33,34] With the solid-state electrolyte, the discharge capacity increased from ≈120 to 140 mAh g^{-1}. The increased robustness of the solid-state cells towards high voltages is noteworthy since elevating the upper cut-off voltage is a straightforward way to increase the energy density.[35] A major increase in capacity was observed when accessing voltage regions below 2.5 V in both the liquid and the solid electrolyte cells. High capacities above 300 mAh g^{-1} were observed in the liquid electrolyte upon further decreasing the lower cut-off voltage to 2.0 and 1.5 V; however, the capacity of liquid electrolyte cells faded rapidly during the three measured cycles. Top-view SEM images show the complete degradation and delamination of the cathode film in cycled cathodes (Figure S2, Supporting Information), indicating that the extra capacity is due to the degradation of the cathode and the liquid electrolyte and not to reversible lithium cycling. In contrast, the solid-state cells show a steady increase from 140 to 300 mAh g^{-1} in the range of 1.5–4.7 V. Cycling at a high capacity of 300 mAh g^{-1} at 1.5–4.7 V and 1 C is possible due to multi-electron cycling. Experiments to further lower the cut-off voltage to 0.8 V for solid-state cells resulted in no remaining discharge capacity after three cycles. To investigate the effect of liquid and solid electrolytes on the capacity, charge–discharge curves of fresh cells over ten cycles at C/2 were recorded for liquid and solid electrolyte cells at 3.0–4.3 V, 3.0–4.7 V, and 1.5–4.7 V voltage windows (Figure 2d–i). The liquid electrolyte cell yielded a capacity above 150 mAh g^{-1} for the first few cycles, which was in accordance with the literature values.[34] The capacity was lower for the solid electrolyte cell since the liquid electrolyte can fill the cracks present in NMC811 after annealing (Figure S2, Supporting Information), while the contact between NMC811 and LiPON is limited to the interface. Upon close inspection, the liquid electrolyte cathode showed faster capacity degradation than the solid electrolyte cell. This accelerated degradation is not surprising since Ni-rich NMC without bulk doping or surface coating strategies is notorious for capacity fading in liquid electrolytes. This behavior is commonly attributed to transition metal dissolution into the liquid electrolyte and side reactions with reactive species originating from liquid electrolytes at elevated voltage.[36] Transition metal dissolution into the liquid organic electrolyte was confirmed by ICP-MS (Figure S3, Supporting Information). In contrast, the solid electrolyte cell (Figure 2g) exhibits no significant overpotential and displays stable cycling. It is essential to note that increasing the upper cut-off voltage from 4.3 to 4.7 V did not significantly increase the capacity for either investigated system. When the lower cut-off voltage was decreased from 3.0 V to 1.5 V, however, the solid-state cells did show an increased capacity of 300 mAh g^{-1}, whereas the liquid electrolyte cell suffered from a large overpotential with a capacity below 200 mAh g^{-1}.

To access the full capacity potential, the Li-rich NMC811 cathodes were cycled at a rate of C/10, a comparatively low rate for thin-film cathodes, resulting in a capacity of 350 mAh g^{-1} for the first cycle (**Figure 3**a). By applying the idea of multi-electron cycling to NMC811, the capacity can be increased from ≈200 to 350 mAh g^{-1}, exceeding the capacity of recently investigated multi-electron Li_2VOPO_4 cathodes.[37] The insertion and extraction of the second lithium can be seen as a bend in the charge–discharge curve and a peak in thee corresponding differential capacity (Figure 3b) at ≈2.0 V and again at 1.6 V. The shape of the charge–discharge curve follows the one observed in chemically and electrochemical overlithiated NMC-type cathodes.[19,38] It is worth noting that at higher C-rates, the charge–discharge curve retains its overall shape (Figures S4 and S5, Supporting Information), albeit with a lower overall capacity. This suggests that only part of the cathode film is cycled beyond one Li per formula unit due to kinetic limitations present at high currents. These results show the importance of accessing voltages below 2.0 V to take advantage of the multi-electron cycling in Li-rich NMC811 cathodes.

Electrochemical impedance spectroscopy was used to investigate the effect of different voltage ranges on the interfacial resistance after running the cells for three cycles between

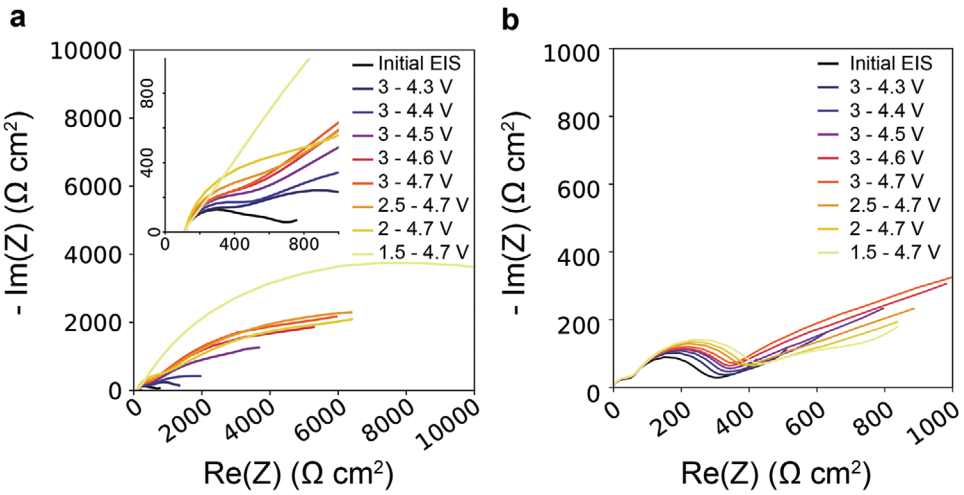

Figure 4. Nyquist plots of the a) liquid and b) solid electrolyte cells after cycling at different voltage ranges.

1.5 and 4.7 V. Fresh cells with the liquid electrolyte displayed an initial impedance above 700 Ω cm^2 (**Figure 4**a). Cycling the cells for three cycles in voltage beyond 3–4.3 V resulted in a increase in resistance to >10 kΩ cm^2. This sharp increase confirmed that the NMC811 cannot cycle with liquid electrolytes in voltage windows beyond 3–4.3 V without interfacial degradation. Two distinctive semicircles were observed for the all-solid-state cells with LiPON as the electrolyte (Figure 4b). The first semicircle, which corresponds to the LiPON solid-state electrolyte and is not affected by increasing voltage, is due to the relatively low ionic conductivity of LiPON (2×10^6 S cm^{-1})[39] compared to the liquid electrolyte conductivity in the mS cm^{-1} range. The second semicircle relates to the charge transfer resistance from the NMC811 cathode to the electrolyte. While the voltage window increased from 3–4.3 V to 1.5–4.7 V, the impedance rose only from 300 Ω cm^2 to below 500 Ω cm^2.These results suggest that the LiPON solid-state electrolyte helps to stabilize the cathode electrolyte interface and to mitigate the impedance increase during cell operation. This effect is reminiscent of those reported for a Li-Nb-O or LiPON coating of active cathode material in bulk cells[27,30,40] or coated multi-electron vanadium-based cathodes.[37]

In a next step, prolonged cycling of thin-film Li-rich NMC811 cathodes in liquid- and solid electrolyte cells was attempted.

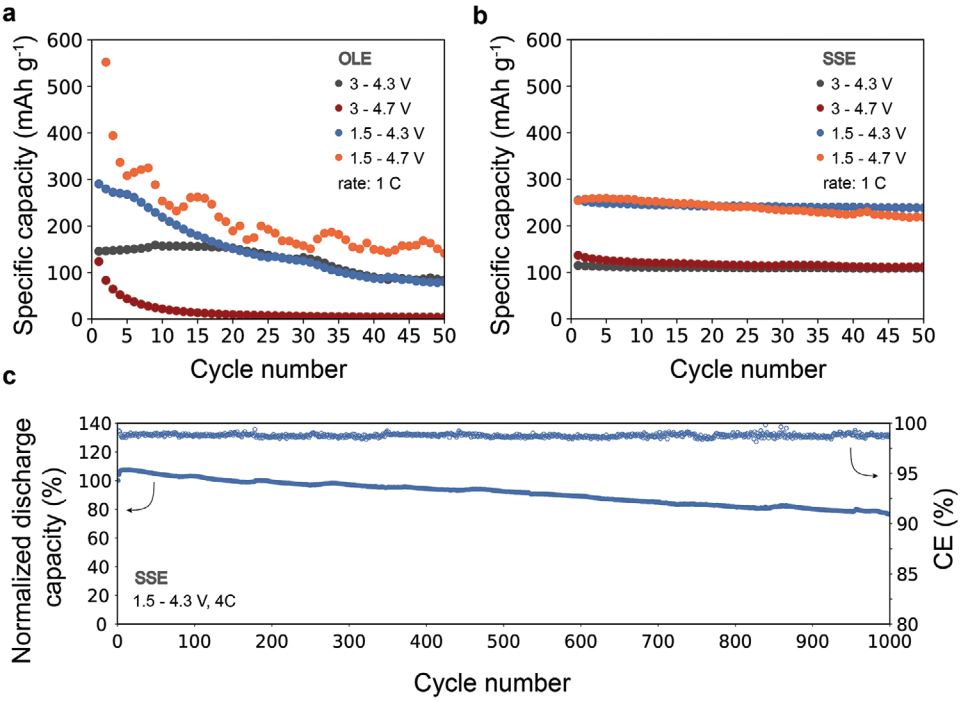

Figure 5. a) First fifty cycles at different voltages in OLE b) First fifty cycles at different voltages in SSE. c) Cycling performance of the SSE cell in the voltage range of 1.5–4.3 V at 4C. The initial capacity at 100% corresponds to 149 mAh g^{-1}.

Li-rich Ni-based cathodes are held back by rapid capacity decay during cycling and in the case of NMC-type cathodes, multi-electron cycling was so far limited to a single cycle.[19,20] Fresh cells for either electrolyte were cycled for 50 cycles at C/2 at 3–4.3 V, 3–4.7 V, 1.5-4.3 V, and 1.5-4.7 V (**Figure 5**a,b). For the liquid electrolyte cell, cycling in the range of 3–4.3 V resulted in a relatively stable capacity of 150 mAh g^{-1}. Operating at low voltages of 1.5 V increased the initial capacity to 300 mAh g^{-1} at 1.5-4.3 V and 600 mAh g^{-1} at 1.5–4.7 V. However, the capacity gained when cycling below 3.0 V faded quickly and no remaining capacity was observed after 20 cycles at 1.5–4.3 V. Similarly, when cycling above 4.3 V in liquid electrolyte, the additional capacity gained faded in the first few cycle and the remaining cycles were close to the cells cycled at 3–4.3 V. This was attributed to cathode degradation, which was further accelerated at high voltage ranges, as indicated by the low coulombic efficiency (Figure S6, Supporting Information) and transition metal dissolution detected in the electrolyte by ICP-MS.

In contrast to the organic liquid electrolyte, LiPON enabled stable cycling at all investigated voltage ranges (Figure 5b). Two capacity regions are visible in Figure 5b, which were determined by the lower cut-off voltages of 3.0 V and 1.5 V. The capacity of ≈250 mAh g^{-1} corresponded to cells cycled down to 1.5 V, while the higher cut-off voltage of 3.0 V resulted in a capacity of 110 mAh g^{-1}. In both cases, the capacity is mostly independent of the upper cut-off voltage. These findings imply that most of the degradation in solid-state cells occurs when cycling up to 4.7 V with only a marginal increase in capacity. On the other hand, the full potential of Li-rich NMC811 can be exploited when cycling as low as 1.5 V instead of only 3.0 V. To test our finding, a new SSE cell was cycled from 1.5 to 4.3 V for 1000 cycles at 4 C, yielding a cycle life of 904 cycles (Figure 5c). It is remarkable that long-term multi-electron cycling is possible for NMC811. The coulombic efficiency (CE) over the 1000 cycles is 98.79%. One thousand cycles at a CE of 98.79% can be sustained because the metallic Li at the anode acts as a reservoir and can compensate for lithium lost in unavoidable side reactions.[41,42] How long lithium-rich NMC811 cycles in conjunction with a Li-metal anode stable is therefore determined by the depletion rate of the Li metal anode as well as the build-up rate of cell impedance. The average capacity loss per cycle is <0.023% over 1000 cycles, indicating a robust interface between Li-rich NMC811 and LiPON. LiPON is well known to be stable against high voltage cathodes allowing for losses per cycle as low as 0.001% over 10'000 cycles.[43]

3. Conclusion

We demonstrated that sputtered NMC811 thin-films are capable of reversible cycling of more than one lithium per formula unit, providing capacities above 300 mAh g^{-1}. It is striking that multi-electron cycling is discovered for such a Ni-rich material because previously, stable cycling of Li-rich oxide cathodes was limited to Mn-rich materials. By cycling Li-rich NMC811 in different voltage windows ranging from 1.5 to 4.7 V, we found that the LiPON solid-state electrolyte stabilizes the NMC811-electrolyte interface and enables reversible cycling. Accessing potentials below 3.0 V more than doubled the discharge capacity, while increasing the potential above 4.3 V mainly accelerated cathode degradation without adding to the discharge capacity. Between 1.5–4.3 V, the cell could be cycled for over 1000 cycles at 4 C with a cycle-life of 904 cycles (80% remaining initial capacity) whereby the initial capacity was 149 mAh g^{-1}. In contrast, the cells with Li-rich NMC811 degraded after the first few cycles if a liquid electrolyte was used. Electrochemical impedance spectroscopy attributed the difference in performance to the stable nature of the NMC811-LiPON interface. These results of a Li-rich NMC811 cathode on a LiPON model electrolyte highlight the importance of reassessing the potential of layered oxide cathode materials when coupled to stable solid-state electrolytes. This work demonstrates that solid-state electrolytes can enable the use of over-lithiated layered cathode materials in solid-state batteries with extended lifetimes and can serve as the basis for future studies on next-generation batteries.

4. Experimental Section

Substrate Fabrication: The base substrate in this study was a heat-resistant ferritic chrome steel foil. To prevent lithium diffusion into the stainless steel substrate during cathode crystallization at 600 °C, a solution-processed ITO layer 180 nm thick was introduced between the substrate and cathode. Details regarding the substrate preparation are provided by Rumpel et al.[44]

For GI-XRD the thin-film NMC811 cathodes were prepared on single-side polished sapphire (0001) wafers (University Wafers). Rigid sapphire was a more favorable substrate for XRD than flexible steel foil. First, the sapphire wafers were coated with a 20 nm Ti adhesion promoter layer and a 300 nm Pt current collector by RF magnetron sputtering. The sputtering deposition was performed from Ti and Pt targets (Plasmaterials Inc.) in an Orion sputtering system (AJA International Inc.), applying a sputtering power of 3 W cm^{-2} at a pressure of 0.3 Pa and 50 sccm Ar gas flow. To limit lithium diffusion into the current collector during cathode crystallisation at 600 °C, a sputtered ITO layer 180 nm thick was introduced between the substrate and cathode. ITO was deposited in a CT200 magnetron sputtering cluster (Alliance Concept) employing a target from Stanford Advanced Materials. The ITO sputtering was carried out with a power of 3.1 W cm^{-2}, a gas flow of 60 sccm Ar + 0.5 sccm O_2, and a chamber pressure of 0.6 Pa.

Cathode Deposition: NMC811 films with a thickness of 600 nm were deposited at room temperature by RF magnetron sputtering in confocal off-axis geometry (AJA International Inc.). An overlithiated NMC811 target ($Li_{1.6}Ni_{0.8}Mn_{0.1}Co_{0.1}O_X$) from Toshima Manufacturing Co. was sputtered in an Orion sputtering system at a pressure of 3 Pa, under a gas flow of 24 sccm Ar + 1 sccm O_2, and with a power density of 5.9 W cm^{-2}. Films were postannealed at 600 °C for 1 h in a tube furnace (Carbolite Gero GmbH & Co.) in an O_2 flow at atmospheric pressure.

All-SSB Fabrication: First, 500 nm LiPON films were deposited on NMC811 cathode films at room temperature by RF magnetron sputtering with a stoichiometric Li_3PO_4 target from Kurt J Lesker Co. at a pressure of 0.4 Pa with N_2 gas flow and with a power density of 5.0 W cm^{-2}. To compensate for lithium loss, Li_2O (Toshima Manufacturing Co.) was cosputtered with a power of 6.0 W cm^{-2}. The conductivity of the LiPON film was 2×10^{-6} S cm^{-1}. Two-micrometre-thick lithium dots were thermally evaporated on top of the LiPON film using an Ångstrom evaporator. The lithium dots were either circular with a diameter of 0.1 cm (area of 0.008 cm^2) or rectangular with dimensions of 0.3 cm by 0.5 cm (area of 0.150 cm^2).

Electrochemical Testing: Electrochemical testing was performed in a three-electrode electrochemical cell with liquid electrolyte. Lithium foil (Sigma–Aldrich) was used as the counter and reference electrode. The electrolyte was propylene carbonate with 1.0 M $LiClO_4$ (Sigma–Aldrich). Cathode loading was calculated using the target density (3.8 g cm^{-3}), the film thickness (600 nm) and the area of the lithium dots or electrochemical cell (0.9 cm^2). The cell setup was clamped on the cathode using a Viton O-ring to seal the aperture. The cell was connected to a Squidstat potentiostat (Admiral Instruments) inside an argon-filled glovebox (Inert Corp.) at 30 °C. After equilibration, electrochemical impedance spectra (EIS) were acquired by charging the cells to 4 V at 1 C (= 40.0 µA cm^{-2}) and then stabilizing the potential until the current was below 1.1 µA cm^{-2}.

Characterization: Crystalline phases were investigated by X-ray diffractometry (Bruker D8 Discover) in grazing-incidence mode using Cu Ka1 radiation at an incident angle of w = 2° and measuring in the range 2*theta* = 10°–80°. Phase identification and Rietveld refinements were performed using open-source Profex software. The composition of the samples was measured by Rutherford back-scattering spectrometry (RBS) and particle induced X-ray emission (PIXE). Measurements were performed with a 2 MeV He beam using a silicon drift diode X-ray detector and a silicon charged particle detector at 168°. The collected RBS data was analysed by the RUMP code. The lithium content was determined by elastic recoil detection analysis (ERDA) with a 13 MeV $^{127}I+$ primary beam and a time-of-flight spectrometer combined with a gas ionization detector.

TOF-SIMS: The 3D chemical structure of the sample was obtained using time-of-flight secondary ion mass spectrometry (TOF-SIMS)[45], one of the very few chemical analysis techniques that allows the detection of lithium at the nanoscale.[46,47] An HV-compatible compact TOF detector (CTOF) from TOFWERK (Thun, Switzerland), with lateral resolution <50 nm, depth resolution <20 nm[48,49] and mass resolution between 700 and 1100 instrument from Tescan (Brno, Czech Republic) was used. A continuous (i.e., not pulsed) monoisotopic $^{69}Ga^+$ primary ion beam was employed for sputtering and analysis (dynamic-SIMS). The 20 keV energy, 112 pA ion current and 12 µs dwell time were used. During the measurement, the beam scanned over a 10 µm×10 µm area with 512 × 512 pixels and 2 × 2 binning. A total of 1395 scans were acquired to obtain information about the entire multilayer sample (i.e., to reach the substrate). Positive ion detection mode was applied and mass calibration was performed using In ion signals. The presented TOF-SIMS data were collected within 74 min. TOF-SIMS Explorer version 1.12.2.0 from TOFWERK was used for data acquisition and processing.

Supporting Information

Supporting Information is available from the Wiley Online Library or from the author.

Acknowledgements

A.A. and J.S. contributed equally to this work. This work was supported by the joint Empa-Fraunhofer ICS project "IE4B" under the ICON funding line and the Swiss National Science Foundation (grant number 200021_172764). The authors acknowledge support from the Scientific Center for Optical and Electron Microscopy (ScopeM) of the Swiss Federal Institute of Technology in Zurich (ETHZ).

Open access funding provided by ETH-Bereich Forschungsanstalten.

Conflict of Interest

The authors declare no conflict of interest.

Data Availability Statement

The data that support the findings of this study are available from the corresponding author upon reasonable request.

Keywords

Li-rich Ni-based cathodes, NMC811, solid-state lithium-ion batteries, thin-films

Received: May 23, 2022
Revised: August 12, 2022
Published online: September 1, 2022

[1] *Global EV Outlook 2020 – Analysis*, https://www.iea.org/reports/global-ev-outlook-2020.
[2] J. Liu, Z. Bao, Y. Cui, E. J. Dufek, J. B. Goodenough, P. Khalifah, Q. Li, B. Y. Liaw, P. Liu, A. Manthiram, Y. S. Meng, V. R. Subramanian, M. F. Toney, V. V. Viswanathan, M. S. Whittingham, J. Xiao, W. Xu, J. Yang, X.-Q. Yang, J.-G. Zhang, *Nat. Energy* **2019**, *4*, 180.
[3] M. S. Whittingham, *Chem. Rev.* **2014**, *114*, 11414.
[4] *Nat. Energy* **2020**, *5*, 825.
[5] C. Mao, R. E. Ruther, J. Li, Z. Du, I. Belharouak, *Electrochem. Commun.* **2018**, *97*, 37.
[6] S. Lee, W. Li, A. Dolocan, H. Celio, H. Park, J. H. Warner, A. Manthiram, *Adv. Energy Mater.* **2021**, *11*, 2100858.
[7] S. Chen, C. Niu, H. Lee, Q. Li, L. Yu, W. Xu, J.-G. Zhang, E. J. Dufek, M. S. Whittingham, S. Meng, J. Xiao, J. Liu, *Joule* **2019**, *3*, 1094.
[8] P. Rozier, J. M. Tarascon, *J. Electrochem. Soc.* **2015**, *162*, A2490.
[9] W. He, W. Guo, H. Wu, L. Lin, Q. Liu, X. Han, Q. Xie, P. Liu, H. Zheng, L. Wang, X. Yu, D.-L. Peng, *Adv. Mater.* **2021**, *n/a*, 2005937.
[10] G. Oh, M. Hirayama, O. Kwon, K. Suzuki, R. Kanno, *Chem. Mater.* **2016**, *28*, 2634.
[11] A. Manthiram, *Nat. Commun.* **2020**, *11*, 1550.
[12] J. Liu, J. Wang, Y. Ni, K. Zhang, F. Cheng, J. Chen, *Mater. Today* **2021**, *43*, 132.
[13] G. Liu, Y. Lu, H. Wan, W. Weng, L. Cai, Z. Li, X. Que, H. Liu, X. Yao, *ACS Appl. Mater. Interfaces* **2020**, *12*, 28083.
[14] H. N. Migeon, M. Zanne, C. Gleitzer, J. Aubry, *J. Mater. Sci.* **1978**, *13*, 461.
[15] M. Tabuchi, N. Kuriyama, K. Takamori, Y. Imanari, K. Nakane, *J. Electrochem. Soc.* **2016**, *163*, A2312.
[16] M. Bianchini, A. Schiele, S. Schweidler, S. Sicolo, F. Fauth, E. Suard, S. Indris, A. Mazilkin, P. Nagel, S. Schuppler, M. Merz, P. Hartmann, T. Brezesinski, J. Janek, *Chem. Mater.* **2020**, *32*, 9211.
[17] M. Bianchini, M. Roca-Ayats, P. Hartmann, T. Brezesinski, J. Janek, *Angew. Chem., Int. Ed.* **2019**, *58*, 10434.
[18] K. Kang, C.-H. Chen, B. J. Hwang, G. Ceder, *Chem. Mater.* **2004**, *16*, 2685.
[19] C. Usubelli, M. M. Besli, S. Kuppan, N. Jiang, M. Metzger, A. Dinia, J. Christensen, Y. Gorlin, *J. Electrochem. Soc.* **2020**, *167*, 080514.
[20] L. Lin, K. Qin, Q. Zhang, L. Gu, L. Suo, Y.-s. Hu, H. Li, X. Huang, L. Chen, *Angew. Chem., Int. Ed.* **2021**, *60*, 8289.
[21] Y. Levartovsky, A. Chakraborty, S. Kunnikuruvan, S. Maiti, J. Grinblat, M. Talianker, D. T. Major, D. Aurbach, *ACS Appl. Mater. Interfaces* **2021**, *13*, 34145.
[22] L. Zou, J. Li, Z. Liu, G. Wang, A. Manthiram, C. Wang, *Nat. Commun.* **2019**, *10*, 3447.
[23] U. Nisar, N. Muralidharan, R. Essehli, R. Amin, I. Belharouak, *Energy Storage Mater.* **2021**, *38*, 309.

[24] A. M. Wise, C. Ban, J. N. Weker, S. Misra, A. S. Cavanagh, Z. Wu, Z. Li, M. S. Whittingham, K. Xu, S. M. George, M. F. Toney, *Chem. Mater.* **2015**, *27*, 6146.
[25] Y. Kim, H. Park, K. Shin, G. Henkelman, J. H. Warner, A. Manthiram, *Adv. Energy Mater.* **2021**, *11*, 2101112.
[26] S. Shrestha, J. Kim, J. Jeong, H. J. Lee, S. C. Kim, H. J. Hah, K. Oh, S.-H. Lee, *J. Electrochem. Soc.* **2021**, *168*, 060537.
[27] S. K. Martha, J. Nanda, Y. Kim, R. R. Unocic, S. Pannala, N. J. Dudney, *J. Mater. Chem. A* **2013**, *1*, 5587.
[28] N. D. Phillip, R. E. Ruther, X. Sang, Y. Wang, R. R. Unocic, A. S. Westover, C. Daniel, G. M. Veith, *ACS Appl. Energy Mater.* **2019**, *2*, 1405.
[29] D. Cheng, T. A. Wynn, X. Wang, S. Wang, M. Zhang, R. Shimizu, S. Bai, H. Nguyen, C. Fang, M.-c. Kim, W. Li, B. Lu, S. J. Kim, Y. S. Meng, *Joule* **2020**, *4*, 2484.
[30] F. Xin, H. Zhou, X. Chen, M. Zuba, N. Chernova, G. Zhou, M. Whittingham, *ACS Appl. Mater. Interfaces* **2019**, *11*, 34889.
[31] J. B. Bates, N. J. Dudney, B. J. Neudecker, F. X. Hart, H. P. Jun, S. A. Hackney, *J. Electrochem. Soc.* **2000**, *147*, 59.
[32] R. Marom, O. Haik, D. Aurbach, I. C. Halalay, *J. Electrochem. Soc.* **2010**, *157*, A972.
[33] H. Hemmelmann, J. K. Dinter, M. T. Elm, *Adv. Mater. Interfaces* **2021**, *8*, 2002074.
[34] N. D. Phillip, R. E. Ruther, X. Sang, Y. Wang, R. R. Unocic, A. S. Westover, C. Daniel, G. M. Veith, *ACS Appl. Energy Mater.* **2019**, *2*, 1405.
[35] W. Li, B. Song, A. Manthiram, *Chem. Soc. Rev.* **2017**, *46*, 3006.
[36] H. Y. Asl, A. Manthiram, *Science* **2020**, *369*, 140.
[37] N. A. Chernova, M. F. V. Hidalgo, C. Kaplan, K. Lee, I. Buyuker, C. Siu, B. Wen, J. Ding, M. Zuba, K. M. Wiaderek, I. D. Seymour, S. Britto, L. F. J. Piper, S. P. Ong, K. W. Chapman, C. P. Grey, M. S. Whittingham, *Adv. Energy Mater.* **2020**, *10*, 2002638.
[38] L. Lin, K. Qin, Q. Zhang, L. Gu, L. Suo, Y.-s. Hu, H. Li, X. Huang, L. Chen, *Angew. Chem., Int. Ed.* **2021**, *60*, 8289.
[39] X. Yu, J. B. Bates, G. E. Jellison, F. X. Hart, *J. Electrochem. Soc.* **1997**, *144*, 524.
[40] A. Aribia, J. Sastre, X. Chen, E. Gilshtein, M. H. Futscher, A. N. Tiwari, Y. E. Romanyuk, *J. Electrochem. Soc.* **2021**, *168*, 040513.
[41] J. Xiao, Q. Li, Y. Bi, M. Cai, B. Dunn, T. Glossmann, J. Liu, T. Osaka, R. Sugiura, B. Wu, J. Yang, J.-G. Zhang, M. S. Whittingham, *Nat. Energy* **2020**, *5*, 561.
[42] P. Albertus, S. Babinec, S. Litzelman, A. Newman, *Nat. Energy* **2018**, *3*, 16.
[43] J. Li, C. Ma, M. Chi, C. Liang, N. J. Dudney, *Adv. Energy Mater.* **2015**, *5*, 1401408.
[44] M. Rumpel, M. Machhaus, J. Sastre, S. Ziegler, X. Chen, A. Flegler, Y. E. Romanyuk, G. A. Giffin, *Mater. Adv.* **2021**, *2*, 2289.
[45] J. C. Vickerman, *Surf. Interface Anal.* **1987**, *10*, 435.
[46] A. Priebe, T. Xie, L. Pethö, J. Michler, *J. Anal. At. Spectrom.* **2020**, *35*, 2997.
[47] A. Priebe, J.-P. Barnes, T. E. J. Edwards, L. Pethö, I. Balogh, J. Michler, *Anal. Chem.* **2019**, *91*, 11834.
[48] J. A. Whitby, F. Östlund, P. Horvath, M. Gabureac, J. L. Riesterer, I. Utke, M. Hohl, L. Sedláček, J. Jiruše, V. Friedli, M. Bechelany, J. Michler, *Adv. Mater. Sci. Eng.* **2011**, *2012*, e180437.
[49] D. Alberts, L. von Werra, F. Oestlund, U. Rohner, M. Hohl, J. Michler, J. A. Whitby, *Instrum. Sci. Technol.* **2014**, *42*, 432.